



# MULTISTABILITY, PHASE DIAGRAMS AND STATISTICAL PROPERTIES OF THE KICKED ROTOR: A MAP WITH MANY COEXISTING ATTRACTORS

LUCIANO CAMARGO MARTINS

*Instituto de Física, Universidade Federal do Rio Grande do Sul,  
91501-970 Porto Alegre, Brazil*

*Departamento de Física, Universidade do Estado de Santa Catarina,  
89223-100 Joinville, Brazil  
lmartins@if.ufrgs.br*

JASON ALFREDO CARLSON GALLAS

*Instituto de Física, Universidade Federal do Rio Grande do Sul,  
91501-970 Porto Alegre, Brazil*

Received December 29, 2006; Revised June 4, 2007

We investigate the prevalence of multistability in the parameter space of the kicked rotor map. We report high-resolution phase diagrams showing how the density of attractors and the density of periods vary as a function of both model parameters. Our diagrams illustrate density variations that exist when moving between the familiar conservative and strongly dissipative limits of the map. We find the kicked rotor to contain multistability regions with more than 400 coexisting attractors. This fact makes the rotor a promising high-complexity local unit to investigate synchronization in networks of chaotic maps, in both regular and complex topologies.

*Keywords:* Phase diagrams; kicked rotor; shrimps; multistability.

## 1. Introduction

One of the most characteristic signatures of dissipative nonlinear systems in Nature is the phenomenon of *multistability*, namely the possibility of observing the coexistence of two or more stationary states, *attractors*, which are stable for a common set of control parameters. Multistability is by no means rare: it appears abundantly in virtually any nonlinear model of physical system. For instance, it is trivial to make the number of coexisting attractors of nonlinear systems to grow beyond any fixed bound by the simple expedient of going to the limit of vanishing dissipation. Moreover, as parameters are tuned, each coexisting state evolves in its characteristic way, some of them eventually losing stability, and some of their unstable partners becoming stable

in a myriad of possible ways via specific *bifurcations* [Arnold *et al.*, 1999].

In spite of a large number of papers devoted to the study of multistability, we believe that the richness of the phase diagrams for many theoretically interesting and experimentally accessible physical systems has not yet been adequately explored, particularly taking into account the complicated structuring of chaotic phases and its many windows of nonchaotic solutions, and, more importantly, for parameters lying far from the Hamiltonian limit. In the present paper we investigate a simple and interesting physical model: a dissipative kicked-rotor. Multistability and complicated basins of coexisting attractors in the dissipative kicked-rotor map have been reported previously by Feudel *et al.* [1996].

However, they focused on the parameter regime where the dissipation is weak. Motivated by their beautiful paper, our aim is to extend their study to considerably broader regions in the parameter space, presenting detailed high-resolution phase diagrams obtained numerically.

A key motivation for undertaking this investigation is a recent work presenting robust numerical evidence that certain synchronization effects commonly observed in lattices of coupled logistic maps are strongly dependent on the local map [Lind *et al.*, 2006]. Specifically, it was shown that coherence may be easily destroyed by simply substituting the *single-atttractor* logistic map by a *bistable* map with two competing chaotic attractors like, e.g. a quartic [Brunnet & Gallas, 1998; Janosi & Gallas, 1999] or a cubic map [Lind *et al.*, 2004a]. This remarkable feature was found to be true not only for *regular* but also in small-world, scale-free and other *complex* network structures, a novel and realistic framework that is attracting much attention in the literature at present [Newman *et al.*, 2006; Watts, 1999; Jost, 2005; Barabási, 2003; Buchanan, 2002; Paula *et al.*, 2006; Lind *et al.*, 2004b]. A number of interesting related questions involving kicked rotors have been discussed recently [Chacon & García-Hoz, 2003; Wimberger, 2004; Persson *et al.*, 2006].

In the context above, an enticing open question is what happens when instead of using local oscillators supporting only a few attractors, like the pair of attractors considered in Refs. [Lind *et al.*, 2006; Brunnet & Gallas, 1998; Janosi & Gallas, 1999; Lind *et al.*, 2004a], one uses maps supporting many, say hundreds, of coexisting attractors? To be able to address this question one first needs to characterize multistability, phase diagrams and the statistical properties of any candidate map having a large number of attractors, to be subsequently used as local oscillator in networks of maps. This characterization is the aim of the present paper. A companion paper will address the problem of synchronization in the presence of a myriad of coexisting attractors [Martins & Gallas, 2008].

As mentioned, the investigation of dynamical systems displaying large numbers of coexisting attractors was considered in an interesting work. Feudel *et al.* [1996] reported that a kicked rotor with a small amount of damping may possess an arbitrarily large number of coexisting periodic attractors when the damping is small enough. In this situation, the large number of stable orbits

yields a complex structure of closely interwoven basins of attraction, whose boundaries fill almost the whole state space. As they explained, most of the attractors observed in the kicked rotor have low periods, because high period stable orbits generally have basins too small to be detected. In a separate work, Feudel *et al.* reported the kicked double rotor to contain more than 3,000 coexisting attractors [Feudel *et al.*, 1998]. The abundance of attractors was conjectured by these authors to be even more pronounced for higher-dimensional systems. Here we also mention a very interesting work by Astakhov *et al.* [2001] which, although not specifically focusing on the number of coexisting attractors, described multistability and complete chaos synchronization in coupled Hénon maps, an invertible system, showing that a single bifurcational mechanism describes both a loss of chaos synchronization and multistability formation.

The pioneering investigation of Feudel *et al.* [1996] presented persuasive arguments for the existence of dozens of coexisting attractors in the kicked rotor. These authors were interested in the limit of very low damping, having investigated the dynamics for a single specific point in the parameter space of the model and discovered the existence of more than 100 coexisting periodic attractors. In the present work we reconsider the dynamics of the kicked rotor investigating the relative abundance of attractors for a very broad parameter region, including the point investigated by Feudel *et al.* [1996], but considering also the region of nonvanishing dissipation. How abundant is multistability when parameters are varied? How abundant are periodic solutions in parameter regions where chaotic dynamics is possible? These are the main questions of interest to us. They need to be answered in order to see how efficient the kicked rotor would be as a local oscillator in networks of maps [Martins & Gallas, 2008].

The paper is organized as follows. In Sec. 2 we define the model and review briefly some of its basic properties. In Sec. 3 we reconsider the dynamics for the same point in parameter space previously considered in a pioneering result by Feudel *et al.* [1996], corroborating their findings and obtaining an additional attractor of period 120. Then, in Sec. 4 we report a computer experiment designed to produce high-resolution phase diagrams of the density of attractors and the density of periods for wide regions of control parameters. Section 5 summarizes

our findings concerning multistability in parameter space of the kicked rotor.

### 2. The Kicked Rotor

The kicked rotor that we investigate is a transformation of the real plane into itself  $f(x, y) : \mathbb{R}^2 \mapsto \mathbb{R}^2$  defined by the equations [Feudel *et al.*, 1996]

$$\begin{aligned} x_{t+1} &= (x_t + y_t) \pmod{2\pi}, \\ y_{t+1} &= (1 - b)y_t + a \sin(x_t + y_t), \end{aligned} \tag{1}$$

where the subindex  $t = 0, 1, 2, \dots$  represents the discrete time ruling the dynamics,  $a$  represents nonlinearity (i.e. the amplitude of the nonlinear forcing) and  $b$  is connected to the energy dissipation of the rotor and varies between 0 (dissipationless Hamiltonian limit) and 1 (very strong dissipation). The dynamics of these two limiting cases is well known [Lichtenberg & Lieberman, 1992; Schmidt & Wang, 1985; Wenzel *et al.*, 1991]. For a given choice  $(a, b)$  of parameters and initial conditions  $(x_0, y_0)$ , iterating Eq. (1) one obtains an *orbit* of the rotor. Our aim here is to classify the abundance of periodic orbits in parameter space. To this end, for a fixed mesh of parameters, we compute and classify all possible orbits as a function of initial conditions for suitable regions in phase space  $x \times y$ .

For  $b > 0$  the map of Eq. (1) contains a *trapping region* [Feudel *et al.*, 1996] in phase space given by  $[0, 2\pi] \times [-y_{\max}, y_{\max}]$ , where  $y_{\max} = a/b$ . Thus, any initial condition inside this region gives origin to an orbit lying entirely inside itself, without any possibility of escaping (i.e. of divergence). Since the parameter  $b$  is tunable from a Hamiltonian ( $b = 0$ ) up to a strongly dissipative limit ( $b = 1$ ), it is clear that the phase space of the system displays changes from being a chaotic sea interspersed with islands of periodicity to the familiar situation where one observes period-doubling cascades routes to chaos.

The period-1 attractors (fixed points)  $(x^*, y^*)$  of Eq. (1) are obtained by solving the system

$$\begin{aligned} x^* &= (x^* + y^*) \pmod{2\pi} \\ y^* &= (1 - b)y^* + a \sin(x^* + y^*) \end{aligned} \tag{2}$$

which gives

$$(x_m^*, y_m^*) = \left( \arcsin \left( -\frac{2mb\pi}{a} \right), -2m\pi \right) \tag{3}$$

for integer  $m$  such that  $|m| \leq a/2b\pi$ . The Jacobian of Eq. (1) is

$$\mathbb{J} = \begin{pmatrix} 1 & 1 \\ \eta & (1 - b) + \eta \end{pmatrix}, \tag{4}$$

where  $\eta \equiv a \cos(x_t + y_t)$ , with determinant  $J = 1 - b$  which depends on  $b$  only, the parameter regulating energy dissipation in the rotor. The eigenvalues of  $\mathbb{J}$  are

$$j_{\pm} = 1 + \frac{\eta - b}{2} \pm \frac{1}{2} \sqrt{(b - \eta)^2 + 4\eta}. \tag{5}$$

For the parameters  $(a, b) = (4, 0.02)$  considered by Feudel *et al.* [1996], we find

$$(x_m^*, y_m^*) = \left( \arcsin \left( -\frac{m\pi}{100} \right), -2m\pi \right) \tag{6}$$

Equation (6), indicates that

$$y^* = 200 \sin(x^*). \tag{7}$$

This curve is indicated by the dashed line in Fig. 1. It contains the fixed points of the map. This figure also contains the 148 attractors listed in Table 1 below and which are discussed in the next section in detail.

Note that, due to the degenerate possibility of orienting rotations, all orbits appear in symmetrical pairs. That is, orbital points obey

$$(x, y) \text{ has a dual } (x', y') \equiv (2\pi - x, -y). \tag{8}$$

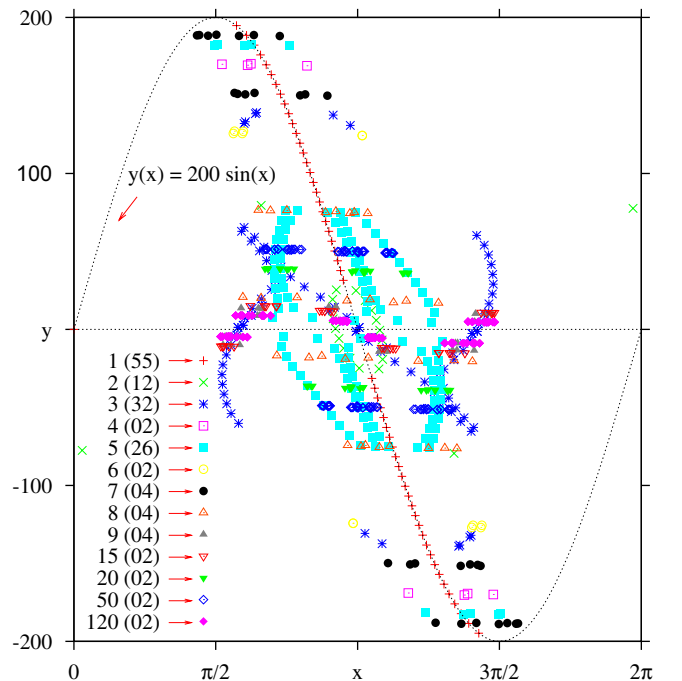


Fig. 1. The 148 attractors found for  $a = 4$  and  $b = 0.02$ , as listed in Table 1 and discussed in Sec. 3. The dashed line defined by Eq. (7) contains all the 55 fixed points.

Table 1. Distribution of periods  $k$  and their respective *degeneracies*  $g_k$  for the 148 attractors found for a mesh of  $3200 \times 3200$  initial conditions. Here  $w_k$  and  $w_k^{\%}$  represent the absolute and relative frequencies of individual periods.

#	$k$	$g_k$	$w_k$	$w_k^{\%}$
1	1	55	549,007	5.35804718
2	2	11	8,128,703	79.33227482
3	3	32	509,075	4.96832986
4	4	2	5,986	0.05842051
5	5	26	935,873	9.13367533
6	6	2	327	0.00319136
7	7	4	1,000	0.00975952
8	8	4	10,414	0.10163569
9	9	4	91,090	0.88899507
10	15	2	8,150	0.07954012
11	20	2	6,184	0.06035290
12	50	2	426	0.00415756
13	120	2	166	0.00162008

### 3. Numerical Experiment: Periodic Attractors for $a = 4$ and $b = 0.02$

For a fixed set of parameters, we determined the periodicity of the asymptotic attractor corresponding to each individual initial condition as follows. First, we discarded  $50 \times 10^3$  iterates, considering them as a transient time needed to come close enough to the asymptotic attractor corresponding to the initial condition used. Then, we determined if the orbit was periodic, taking into account all periods up to a maximum period  $p_{\max} = 1500$ . A point  $(x_t, y_t)$  was considered as belonging to a period- $k$  orbit if  $k$  was the smallest integer such that, for all points of the orbit, we had

$$\|\mathbf{x}_{t+k} - \mathbf{x}_t\| < \epsilon_d, \quad (9)$$

where  $\epsilon_d$  is a small number representing the numerical accuracy of the test. We checked the stability of the numerical assignment of each period by repeating computations using  $\epsilon_d = 10^{-d}$ , for  $d = 7, 8, \dots, 12$ . The results obtained were found to be independent of  $\epsilon_d$ . These strict tests were particularly important in the limit of low-dissipation, when multistability proliferates. In addition, we performed a number of additional tests, for specific parameter sets, using the arbitrary precision package of MAPLE.

To estimate the number of coexisting periodic orbits, we covered the trapping region

$[0, 2\pi] \times [-200, 200]$ , with grid of  $N \times N$  equally spaced initial conditions where

$$N = \{100, 200, 400, 800, 1600, 3200\}.$$

The trapping region considered here is the same one considered by Feudel *et al.* [1996]. To discriminate distinct attractors of the same period, for each orbit we constructed a look-up table containing the particular orbital point, say  $(x_m, y_m)$ , characterized by having the maximum magnitude of  $y_m$ . In this way, comparing these reference points it was possible to discriminate with a precision  $\epsilon$  if two orbits were identical or not.

For the smallest grid ( $N = 100$ ) we detected a total of 114 distinct attractors involving eight different periods:  $\{1, 2, 3, 5, 8, 9, 15, 20\}$ . For  $N = 200$  and larger values, in addition to the eight periods previously found, we also detected orbits with periods  $\{4, 6, 7, 50, 120\}$ , giving now a total of 13 different periods. It is clear that the total number of periodic orbits depends on the resolution of the grid of initial conditions used to cover the trapping region in phase space. For grids larger than  $N = 200$  we have not observed any additional period, indicating that if additional periods exist, their basins must be of rather small volume. For the largest grid,  $N = 3200$  we counted 148 distinct attractors distributed in 13 different periods, the same ones found already for  $N = 200$ . Table 1 summarizes the statistics found for the largest grid  $N = 3200$ . The great majority is of period-2 and period-5 orbits. The small percentage of the orbits with higher periods is a measure of the volume of their basins of attraction.

The distribution of periodic orbits shown in Table 1 confirms the distribution previously determined by Feudel *et al.* [1996], with one exception: we find an additional attractor of period 120, which may be observed at relatively low resolution, despite its small basin of attraction. Another difference is that while Feudel *et al.* [1996] report finding 84.4% of the initial conditions to lead to period-1 orbits, our corresponding number is 5.35%. We obtain a number close to theirs, namely 84.7%, only when adding orbits of period-1 and period-2 together. One additional difference observed with respect to the work of Feudel *et al.* [1996] is connected with period-1 orbits. The 5% of period-1 orbits listed in our Table 1, we observed that the convergence to period-1 is very slow and not perfect, meaning that differences of the order of  $\epsilon$  seem to be always present. For  $\epsilon = 10^{-12}$  the

basin volume of period-1 orbits drops to 4.2% while that corresponding to period-2 orbits increases to 80.3%. Increasing the transient and decreasing the value of  $\epsilon$ , the volume of the period-1 basin further decreases. This was tested for, e.g.  $\epsilon$  from  $10^{-7}$  to  $10^{-12}$ ), with transients of  $100 \times 10^3$  iterates.

Figure 2 shows the *stability “blades”* corresponding to the several possible values of  $m$  obeying  $|m| \leq a/(2b\pi) \simeq 31.8$ , in Eq. (3). As the figure indicates, the point  $(a = 4, b = 0.02)$  is located inside the stability region of the fixed points for which  $|m| = 5, 6, 7, \dots, 31$ , a total of  $2 \times 27 = 54$  points, plus the fixed point for  $m = 0$ , giving a total of 55 points as listed in Table 1.

Figure 3 displays the region in phase space that contains nine of the coexisting period-2 orbits. Our figure contains the domain shown in Fig. 2 of [Feudel *et al.*, 1996] but with higher resolution. In addition to period-2 orbits, the phase-space window shown in Fig. 3 contains orbits of periods other than period-2, for instance, it contains period-1 orbits living inside the large basins denoted  $f$  and  $f'$ . Primed and unprimed pairs of basins refer to pairs of isoperiodic orbits which are conjugate to each other under the symmetry operation defined in Eq. (8). Note that the orbit

living inside the central basin is *self-conjugate*, as indicated.

The box seen in Fig. 3 is shown magnified in Fig. 4(a). The main purpose of Fig. 4 is to illustrate the complex entangling in phase-space generated by the coexistence of several distinct orbits. The successive magnifications serve to indicate the localization and relative size of the period-120 orbit, an orbit apparently not recorded by Feudel *et al.* [1996]. In Fig. 4, period-120 orbital points are marked with the symbol “o”. As indicated by the numbering inside the figure, inside the last few magnifications one finds only attractors with periods 3, 9 and 120, in basins with volumes given by 54%, 29%, 17%, for the penultimate and 33%, 18%, 49%, for the last magnification, respectively.

In the trapping region, one finds two flavors of the period-120 attractor, as dictated by the symmetry with respect to the orientation of the initial rotation, as discussed above. One orbit contains the point  $A = (1.86580061, 8.90035987)$  while its symmetric dual contains the point  $\bar{A} = (4.41738470, -8.90035987)$ , both determined as described above, on a  $1600 \times 1600$  grid of initial conditions. In this grid, of a total of 2,563,201 initial conditions, 42 of them lead to period-120 orbits,

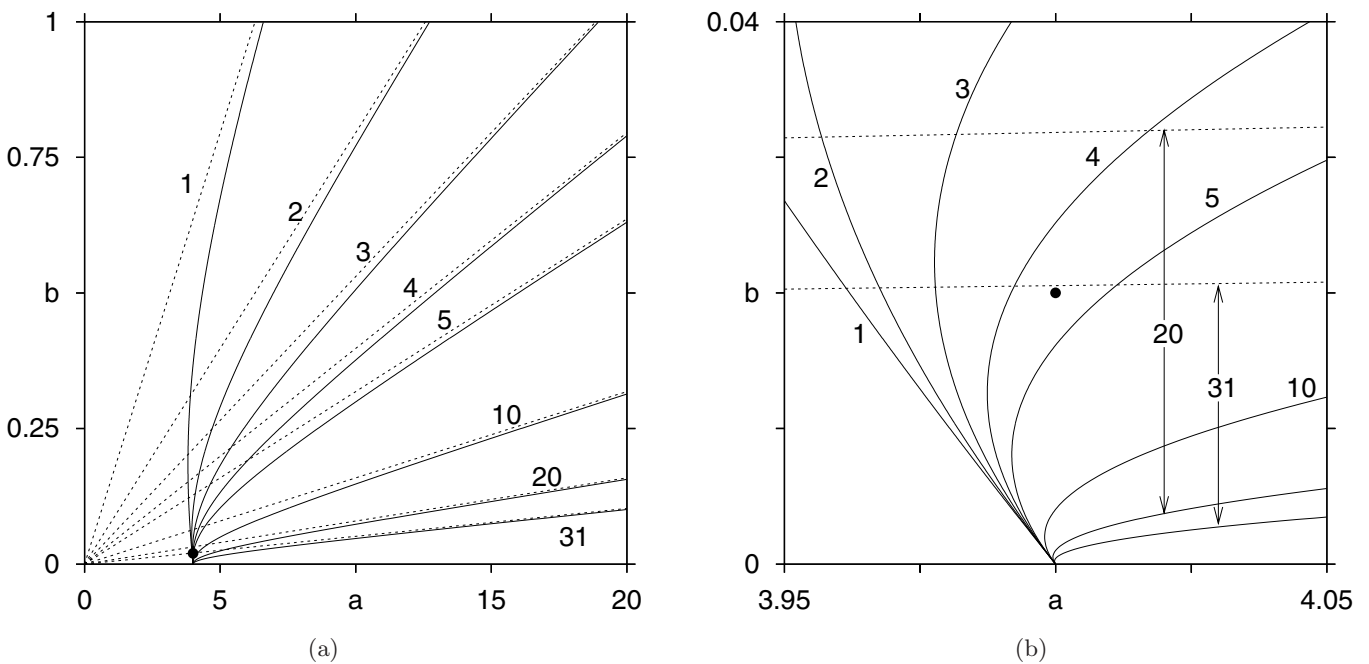


Fig. 2. (a) The stability regions of the fixed points of the rotor. Dotted lines correspond to eigenvalues +1, while the continuous lines mark eigenvalues  $-1$ . (b) Magnification of the region containing the point  $(a = 4, b = 0.02)$ , indicated by a black dot. For reference, the arrows indicate the width of two stability windows. Altogether, there are 55 stable fixed points for this parameter point.

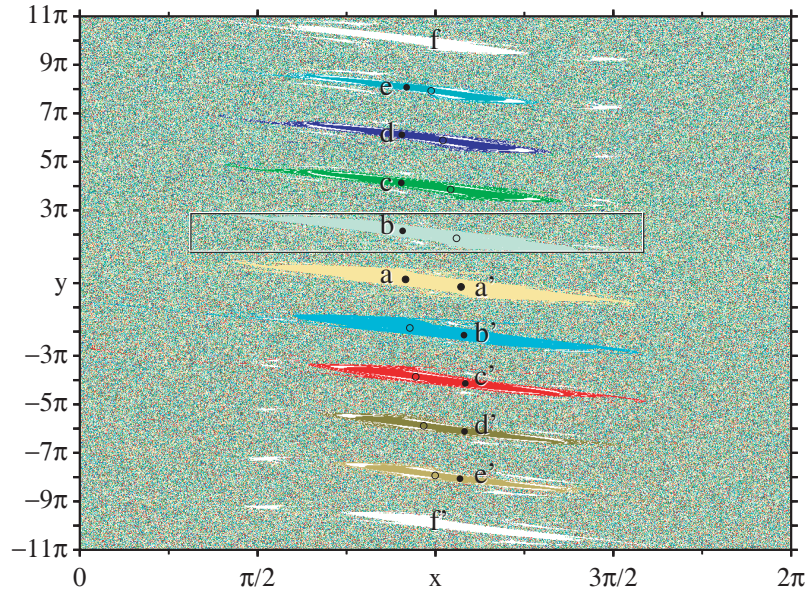


Fig. 3. Region of phase space where 83.8% of the initial conditions lead to five dual pairs of period-2 orbits indicated by the colors. As indicated, the orbit  $a$  is self-dual. Non period-2 orbits are painted white. The big  $f$  white island has period-1. Primes refer to the duality defined in Eq. (8). The coordinates of the full dots are given in Table 2.

19 of them landing in attractor  $A$  and 23 landing in attractor  $\bar{A}$ . The Lyapunov spectra of both attractors is the same:  $\lambda_{\{1,2\}} = \{-0.2659, -0.5963\}$ .

Figure 5 illustrates details of the larger portions of the unprimed basins of periods 1 and 2 of

Fig. 3. The labels  $a, b$ , etc. refer to similar labels also used in Fig. 3. As also noticed by Feudel *et al.* [1996], an interesting feature of these basins is that they seem to have fractal boundaries spreading over most of the phase space, as indicated by the seas

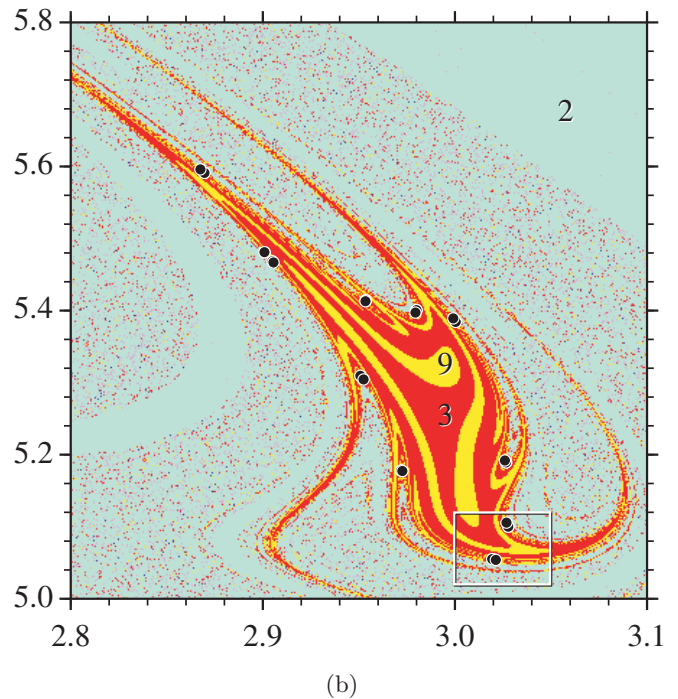
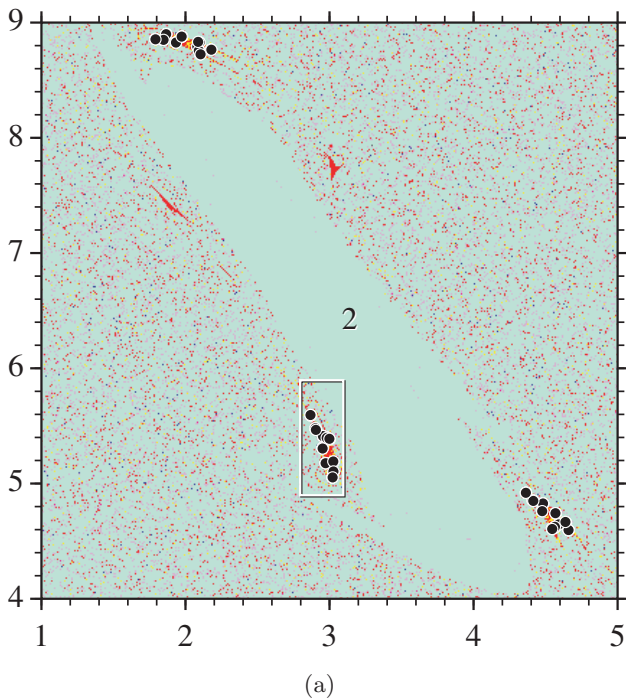
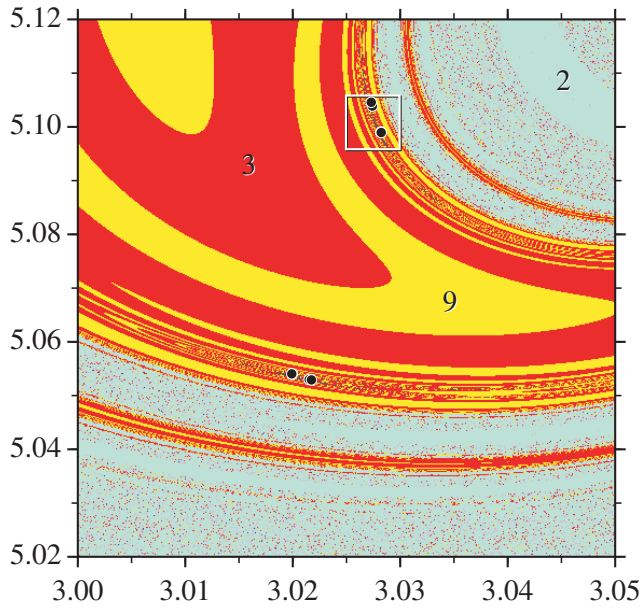
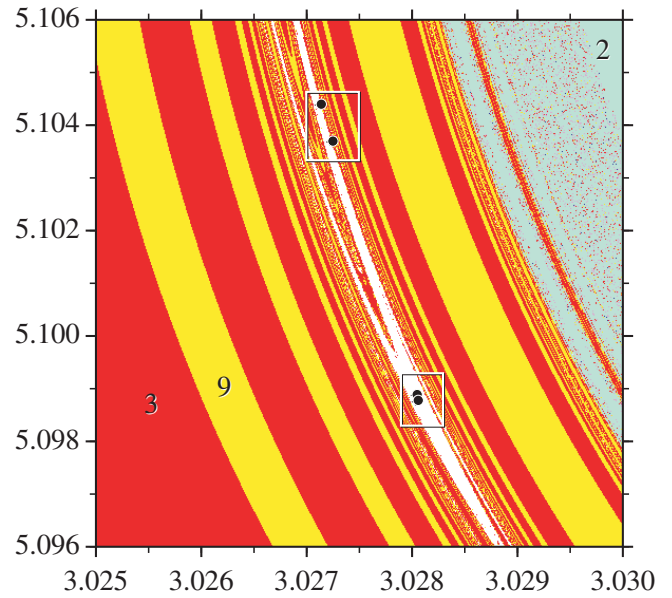


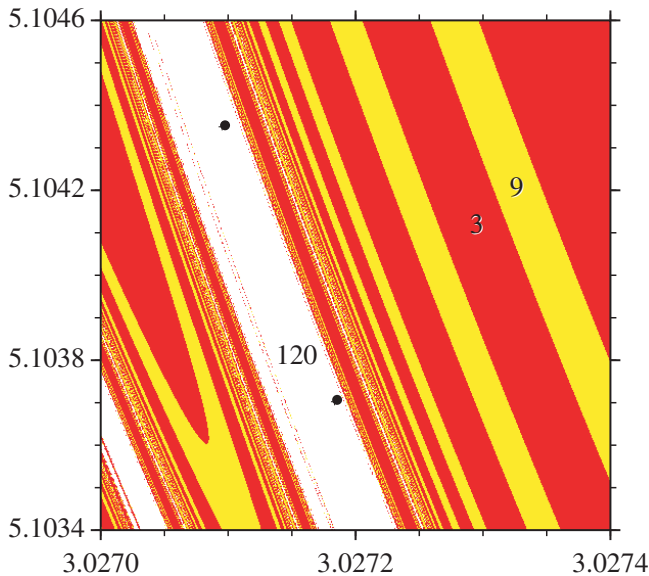
Fig. 4. Successive enlargements show in white the location of the basin and points of the period-120 orbit, indicated by the dots. The two dots in the last panel indicate period-120 points with coordinates  $(3.02803, 5.09887)$  and  $(3.02804, 5.09876)$ .



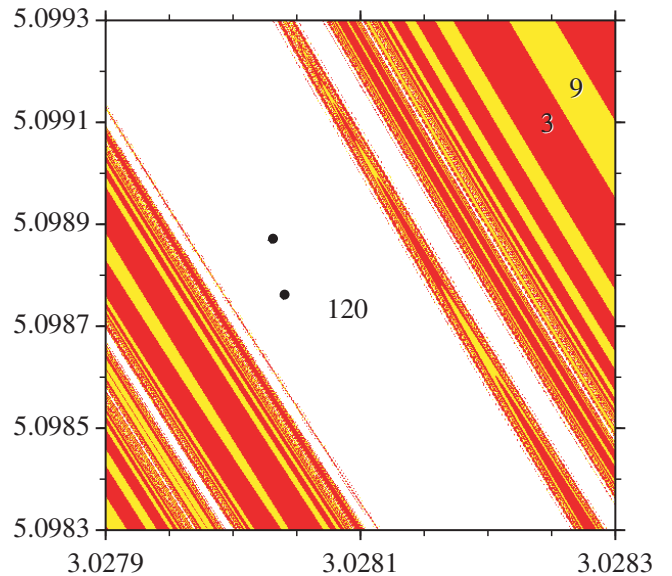
(c)



(d)



(e)



(f)

Fig. 4. (Continued)

of colored dots surrounding the larger connected portions of the basins. Furthermore, note that the colorful sea of points in Fig. 3(c) seems to contain more green, Fig. 3(e) seems to contain more blue, etc., apparently indicating that the color of the large connected domain dominates the coloring of the sea surrounding it.

Table 2 summarizes data discriminating and characterizing the nine coexisting period-2 orbits

together with their Lyapunov spectra, computed for the window in phase space shown in Figs. 3 and 5.

For the record, we mention that our numerical computations were done with 18 to 20 significant digits and floating point variables involving 80 bits of precision. In other words, we used variables of type *extended* according to the IEEE Standard 754 norm, commonly implemented in most computers nowadays.

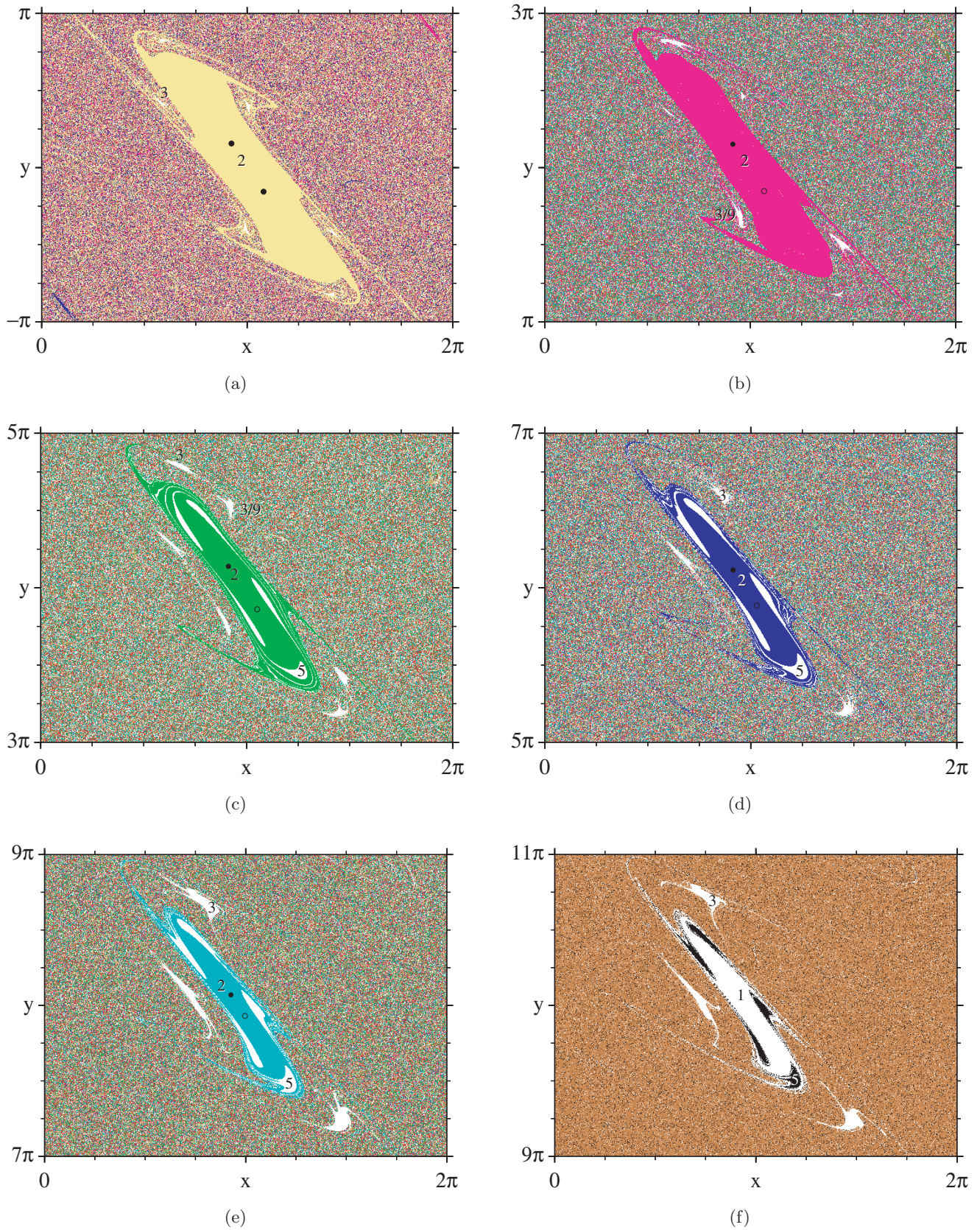


Fig. 5. Magnifications of the larger portions of the periods 1 and 2 shown in Fig. 3. Note the conspicuous presence of period-5 basins attached to the large connected portion of the basins of period-1 and 2. The labeling 3/9 in Fig. 5(c) is the same region depicted in detail in Fig. 3, containing periods 3, 9 and 120. The coordinates of the full dots are given in Table 2. In panel *f* we use black to distinguish period-5 from period-1.

Table 2. Absolute and relative abundance of the nine period-2 orbits contained in the window shown in Fig. 3. There is one additional pair of period-2 orbits, counted in Table 1, located outside the window in Fig. 3. Coordinates  $x_m$ ,  $y_m$  and the Lyapunov exponents to each attractor are shown in the last four columns, respectively. The orbit labeled  $a$  is self-symmetric under the operation defined in Eq. (8).

Attractor	$w$	$w\%$	$x_m$	$y_m$	$\lambda_1$	$\lambda_2$
$a \equiv a'$	212,790	22.17	2.89627484	0.49063562	-0.1242	-0.1242
$b$	150,525	15.68	2.87039114	6.76090914	-0.1216	-0.1216
$b'$	151,250	15.77	3.41279417	-6.76090914	-0.1216	-0.1216
$c$	79,584	8.29	2.85861680	13.00350704	-0.1122	-0.1129
$c'$	81,458	8.48	3.42456851	-13.00350704	-0.1122	-0.1129
$d$	46,882	4.88	2.86507611	19.21068402	-0.0949	-0.0964
$d'$	48,121	5.01	3.41810920	-19.21068402	-0.0949	-0.0964
$e$	16,608	1.73	2.90545180	25.35150612	-0.0615	-0.0624
$e'$	17,507	1.82	3.37773350	-25.35150612	-0.0615	-0.0624
Total	804,726	83.8%	—	—	—	—

#### 4. Phase Diagrams for Arbitrary Parameters

The useful discovery of more than 100 attractors for the kicked rotor by Feudel *et al.* [1996] discussed in the previous section left us wondering how complex would be the parameter space of the rotor as one moves away from the Hamiltonian limit, diving more into the strongly dissipative region of the map. In the dissipationless  $b = 0$  limit the map reduces to the standard map studied many years ago [Zaslavsky, 1978; Chirikov, 1979] while for  $b = 1$  one has the circle map displaying period-doubling cascades to chaos. Although the dynamics in phase-space of the kicked rotor are well-known, its parameter space is by far much less investigated. How does the parameter space of a dynamical system ruled by a transcendental function, like the kicked rotor in the interval  $0 \leq b \leq 1$ , compare with that of a simple polynomial map like, e.g. the Hénon map [Gallas, 1993, 1994, 1995] in  $-1 \leq b \leq 1$ , or even in the smaller orientation-preserving or orientation-reversing intervals [Endler & Gallas, 2006a, 2006b]? Is it possible to find the same characteristic bifurcation rigidity [Hunt *et al.*, 1999] found in polynomial maps for the transcendental equation of motion of the rotor? In this section we present numerical evidence showing that the phase diagram of the rotor in fact displays the same structure as the paradigmatic examples mentioned.

Figure 6 displays the results of an experiment designed to sample the number of distinct attractors over a wide range in parameter space:  $a \in [0, 10]$  and  $b \in [0, 1]$ . This region was discretized with a grid of

$1000 \times 1000$  parameter points. For each of them we determined numerically the number of attractors, the number of distinct periods, thereby obtaining the maximal period and the most frequent period for the grid. For each of the  $10^6$  parameter points we compared and counted attractors, sampled for 2500 initial conditions on a grid of  $50 \times 50$  points covering the trapping region. This long and sensitive computation led to Fig. 6. This figure shows a remarkably high concentration of distinct attractors in the rectangle located roughly at  $a \in [1, 5]$  and  $b \in [0, 0.1]$ . The maximum number of attractors occurring for  $(a, b) = (3, 0.002)$  were counted as 404 distinct attractors. The location of this point is indicated by a cross in Fig. 6. As one moves upward toward  $b = 1$  the density of attractors diminishes considerably. In addition, about half of the parameter window is white, indicating the presence of chaotic attractors.

As indicated by the pair of boxes in Fig. 6, embedded in the chaotic region, it is possible to find a myriad of islands of stability with the general structure of a *shrimp* [Gallas, 1993, 1994, 1995, Hunt *et al.*, 1999], a generic structure also found in profusion in the parameter space of dynamical systems ruled by systems of nonlinear differential equations [Bonatto *et al.*, 2005; Bonatto & Gallas, 2007, 2008; Freire *et al.*, 2008a; Zou *et al.*, 2006]. The larger box, containing an isolated and fat shrimp of period-4 is shown in Fig. 7. In sharp contrast with other two-parameter maps like the Hénon map, for instance, this region is characterized by a very strong compression of stability islands, making them all barely visible in the scale of the figure and

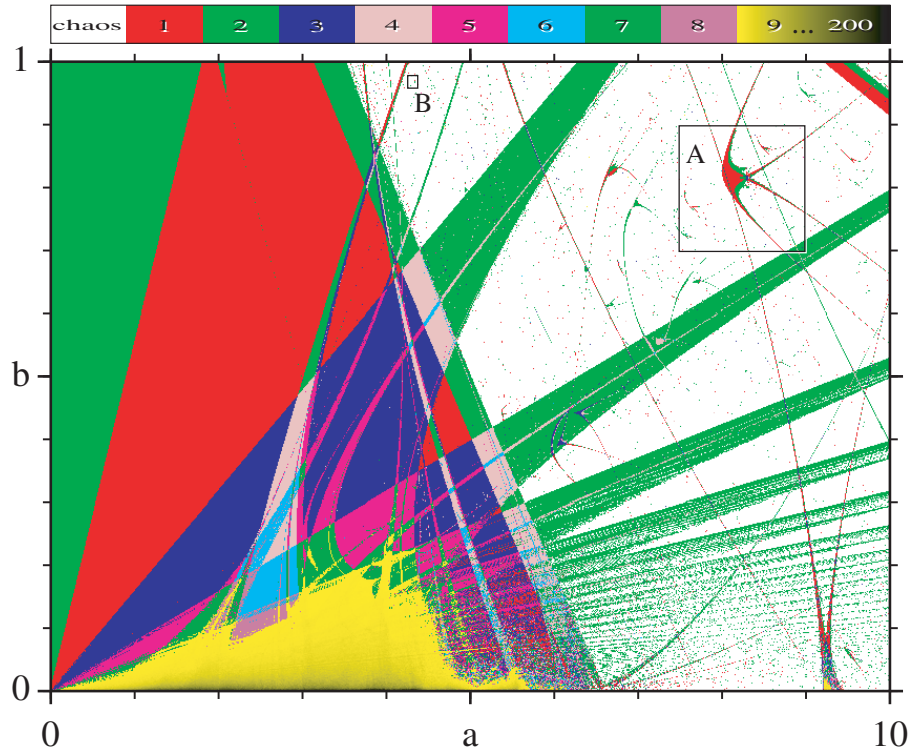


Fig. 6. Density of attractors estimated at each point  $(a, b)$  from a random sampling involving 2500 uniformly initial conditions in the trapping region in phase space discretized on a  $50 \times 50$  grid. The white background, indicated as period 0 in the table of colors, is used to mark chaotic attractors. For points with nine or more attractors, a continuous palette ranging from yellow to black is used. The larger box is shown magnified in Fig. 7 while the smaller box near  $(a, b) \sim (4.3, 0.96)$  is magnified in Fig. 8.

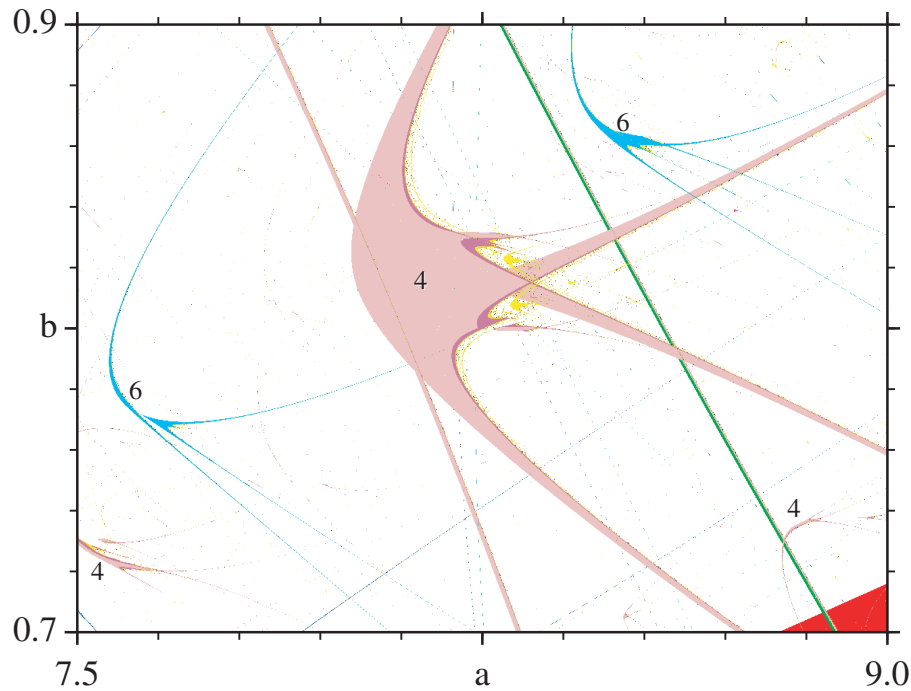


Fig. 7. Magnification of the larger box in Fig. 6, showing regions of periodic behaviors embedded in the white background denoting chaos. The colors indicate the periods characterizing the different islands. Period zero is used to denote chaos. The main body of the larger shrimp is a period-4 region. Its two neighbors have main bodies of period six.

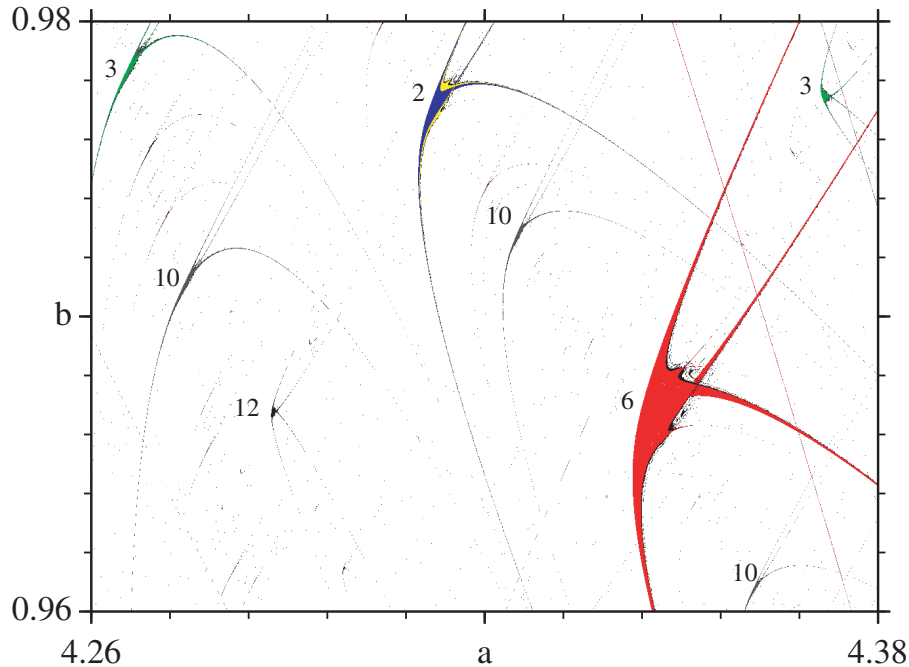


Fig. 8. Magnification of the smaller box indicated in Fig. 6, containing additional *shrimps* similar to those in Fig. 7. The shrimp of largest volume has period 6. Colors denote periods, not density of attractors.

without a suitable sampling of the initial conditions. Figure 8 shows a magnification of the smaller box which is barely visible in Fig. 6. While the shape and distribution of stability islands in this region resemble that of other maps [Gallas, 1993, 1994, 1995; Hunt *et al.*, 1999], it is very distinct in two aspects: the nucleation of stability inside the chaotic region occurs when approaching the strongly dissipative region and, the sequence of periods nucleating along specific lines is rather unusual [Bonatto *et al.*, 2005; Bonatto & Gallas, 2007, 2008], involving main periods 3, 7, 8, 10 and 16, as shown in the figure.

From Fig. 6, one sees that there is a large number of distinct orbits having the same period. It would be interesting to investigate how all these isoperiodic orbits evolve and die as  $b$  moves from the Hamiltonian to the strongly dissipative limit.

## 5. Summary and Outlook

In this work we reconsidered the kicked rotor map shown by Feudel *et al.* [1996] to contain more than hundred attractors in the very low dissipation limit, for  $(a = 4, b = 0.02)$ . We reported high-resolution phase diagrams showing prevalence of multistability and identifying how the density of attractors

varies as a function of both model parameters when moving between the familiar conservative and the strongly dissipative limits of the map. We find the kicked rotor to contain multistability regions with more than 200 coexisting attractors. As far as we know, this is the first time that a detailed and systematic high-resolution phase diagram quantifying density of attractors is reported for parameters far from the low-dissipation limit. As one moves toward the Hamiltonian limit, a remarkable feature observed is that it is the degeneracy of the low-period orbits that increases, not so much the length of the stable periods.

As an interesting application of the phase diagrams obtained here we mention the study of synchronization properties in networks of chaotic systems. Synchronization of chaotic systems has been frequently studied nowadays because of its relevance in applications, e.g. in nonlinear optics and fluid dynamics [Boccaletti *et al.*, 2002]. Very recently, the investigation of synchronization is attracting renewed attention because of its key role in helping to understand the ubiquitous complexity found in the theory of *networks* of all kinds, such as the Internet, the World Wide Web, social, and biological networks, etc. [Newman *et al.*, 2006; Watts, 1999; Jost, 2005]. The main point of these investigations is to consider increasingly realistic couplings

between chaotic local units. For instance, to consider the effect of finite-time propagation of the interaction, particularly of time-delayed coupling [Atay & Jost, 2004; Masoller & Martí, 2005; Martí *et al.*, 2006]. Delayed coupling was used to study the emergence of multistability in noisy bistable elements [Huber & Tsimring, 2003] and to analyze anticipating synchronization of two excitable systems [Ciszak *et al.*, 2004]. It is already known that for continuous-time systems, the stability conditions of coupled elements is not influenced by the time-delay of the coupling when the elements are randomly coupled [Jirsa & Ding, 2004], and that synchronization is independent of the topology but depends on the average number of neighbors [Masoller & Martí, 2005; Martí *et al.*, 2006]. For discrete-time systems modeled by coupled map lattices, it was found that even with random delays, for adequate coupling strength an array of chaotic logistic maps is able to synchronize [Masoller & Martí, 2005].

In this context, we observe that before embarking on applications of multistability of maps one needs first to chart parameter space, building phase diagrams and considering the basin size evolution between dissipative and conservative limits [Rech *et al.*, 2005]. This need is not so directly transparent in the existing literature because the overwhelming majority of papers dealing with networks of coupled maps use the logistic map as a local oscillator, an exceptionally simple map that contains only a single finite attractor (i.e. deal with a map which shows no multistability). We also mention that, instead of dealing with maps involving transcendental functions in their definition, it seems that higher-dimensional maps defined by algebraic functions and displaying multistability, like the Hénon map investigated by Astakhov *et al.* [2001], present less computational complications and pitfalls. At any rate, knowledge of detailed phase diagrams offers now the possibility of exploiting more flexible local oscillators as appealing high-complexity local units to characterize synchronization of chaotic maps in more realistic scenarios, discrete or not [Freire & Gallas, 2007; Freire *et al.*, 2008b], in regular and complex topologies, with or without time-delay among individual units [Martins & Gallas, 2008].

## Acknowledgments

L. C. Martins thanks CNPq (Conselho Nacional de Pesquisa Científica, Brazil) for a Doctoral

Fellowship. J. A. C. Gallas thanks CNPq for a Senior Research Fellowship. This work is supported by the Air Force Office of Scientific Research, contract FA9550-07-1-0102.

## References

- Arnold, V. I., Afrajmovich, V. S., Ilyashenko, Yu. S. & Shilnikov, L. P. [1999] *Bifurcation Theory and Catastrophe Theory* (Springer, Berlin).
- Astakhov, V., Shabunin, A., Uhm, W. & Kim, S. [2001] “Multistability formation and synchronization loss in coupled Hénon maps: Two sides of the single bifurcational mechanism,” *Phys. Rev. E* **63**, 56212.
- Atay, F. M. & Jost, J. [2004] “Delays, connection topology, and synchronization of coupled chaotic maps,” *Phys. Rev. Lett.* **92**, 144101.
- Barabási, A.-L. [2003] *Linked* (Plume, NY).
- Boccaletti, S., Kurths, J., Osipov, G., Valladares, D. L. & Zhou, C. S. [2002] “The synchronization of chaotic systems,” *Phys. Rep.* **366**, 1–101.
- Bonato, C., Garreau, J. C. & Gallas, J. A. C. [2005] “Self-similarities in the frequency-amplitude space of a loss-modulated CO<sub>2</sub> laser,” *Phys. Rev. Lett.* **95**, 0143905.
- Bonato, C. & Gallas, J. A. C. [2007] “Accumulation horizons and period adding in optically injected semiconductor lasers,” *Phys. Rev. E* **75**, 055204(R).
- Bonato, C. & Gallas, J. A. C. [2008] “Accumulation boundaries: Codimension-two accumulation of accumulations in phase diagrams of semiconductor lasers, electric circuits, atmospheric and chemical oscillators,” *Philos. Trans. R. Soc. Series A* **366**, 505–517.
- Brunnet, L. G. & Gallas, J. A. C. [1998] “Exploring collective behaviors with a multi-attractor quartic map,” *Physica A* **257**, 329–333.
- Buchanan, M. [2002] *Nexus: Small World and the Ground-Breaking Theory of Networks* (W. W. Norton, NY).
- Chacon, R. & García-Hoz, A. M. [2003] “Well-behaved dynamics in a dissipative nonideal periodically kicked rotator,” *Phys. Rev. E* **68**, 066217.
- Chirikov, B. V. [1979] “Universal instability of many-dimensional oscillator systems,” *Phys. Rep.* **52**, 265–379.
- Ciszak, M., Marino, F., Toral, R. & Balle, S. [2004] “Dynamical mechanism of anticipating synchronization in excitable systems,” *Phys. Rev. Lett.* **93**, 114102.
- Endler, A. & Gallas, J. A. C. [2006a] “Reductions and simplifications of orbital sums in a Hamiltonian repeller,” *Phys. Lett. A* **352**, 124–128.
- Endler, A. & Gallas, J. A. C. [2006b] “Conjugacy classes and chiral doublets in the Hénon Hamiltonian repeller,” *Phys. Lett. A* **356**, 1–7.

- Endler, A. & Gallas, J. A. C. [2006c] “Mandelbrot-like sets in dynamical systems with no critical points,” *Comptes Rendus Acad. Sci.* **342**, 681–684.
- Feudel, U., Grebogi, C., Hunt, B. R. & Yorke, J. A. [1996] “Map with more than 100 coexisting low-periodic attractors,” *Phys. Rev. E* **54**, 71–81.
- Feudel, U., Grebogi, C., Poon, L. & Yorke, J. A. [1998] “Dynamical properties of a simple mechanical system with a large number of coexisting periodic attractors,” *Chaos Solit. Fract.* **9**, 171–180.
- Freire, J. G. & Gallas, J. A. C. [2007] “Synchronization and predictability under rule 52, a cellular automaton reputedly of class 4,” *Phys. Lett. A* **366**, 25–29.
- Freire, J. G., Bonatto, C., daCamara, C. & Gallas, J. A. C. [2008a] “Intransitivity diagrams for the Lorenz-84 low-order atmospheric circulation model,” *Chaos*, in print.
- Freire, J. G., Brison, O. J. & Gallas, J. A. C. [2008b] “Spatial updating, spatio-temporal transients, and regularities of a complex automaton with nonperiodic architecture,” *Chaos* **17**, in print.
- Gallas, J. A. C. [1993] “The structure of the parameter space of the Hénon map,” *Phys. Rev. Lett.* **70**, 2714–2717.
- Gallas, J. A. C. [1994] “Dissecting shrimps: Results for some one-dimensional physical systems,” *Physica A* **202**, 196–223.
- Gallas, J. A. C. [1995] “The structure of the parameter space of a ring cavity,” *Appl. Phys. B* **60**, S203–S213; Available online at <http://www.if.ufrgs.br/~jgallas>.
- Hunt, B., Gallas, J. A. C., Grebogi, C., Yorke, J. A. & Koçak, H. [1999] “Bifurcation rigidity,” *Physica D* **129**, 35–56.
- Huber, D. & Tsimring, L. S. [2003] “Dynamics of an ensemble of noisy bistable elements with global time delayed coupling,” *Phys. Rev. Lett.* **91**, 260601.
- Janosi, I. M. & Gallas, J. A. C. [1999] “Globally coupled multiattractor maps: Mean-field dynamics controlled by the number of elements,” *Phys. Rev. E* **59**, R28–R31.
- Jirsa, V. K. & Ding, M. [2004] “Will a large complex system with time delays be stable?” *Phys. Rev. Lett.* **93**, 070602.
- Jost, J. [2005] *Dynamical Systems* (Springer, NY), Chapter 8.
- Lichtenberg, A. J. & Leiberman, M. A. [1992] *Regular and Chaotic Dynamics* (Springer-Verlag, NY).
- Lind, P. G., Gallas, J. A. C. & Herrmann, H. J. [2004a] “Coherence in scale-free networks of chaotic maps,” (condmat 0407806) *Phys. Rev. E* **70**, 056207.
- Lind, P. G., Titz, S., Kuhlbrodt, T., Corte-Real, J., Kurths, J., Gallas, J. A. C. & Feddel, U. [2004b] “Coupled bistable maps: A tool to study convection parameterization in ocean models,” *Int. J. Bifurcation and Chaos* **14**, 999–1015.
- Lind, P. G., Nunes, A. & Gallas, J. A. C. [2006] “Impact of bistability in the synchronization of chaotic maps with delayed coupling and complex topologies,” *Physica A* **371**, 100–103.
- Martí, A. C., Ponce, M. & Masoller, C. [2006] “Chaotic maps coupled with random delays: Connectivity, topology, and network propensity for synchronization,” *Physica A* **371**, 104–107.
- Martins, L. C. & Gallas, J. A. C. [2008], work in progress.
- Masoller, C. & Martí, A. C. [2005] “Random delays and the synchronization of chaotic maps,” *Phys. Rev. Lett.* **94**, 134102.
- Newman, M. E. J. & Watts, D. J. [1999] “Scaling and percolation in the small-world network model,” *Phys. Rev. E* **60**, 7332–7342.
- Newman, M. E. J., Barabasi, A.-L. & Watts, D. J. [2006] *The Structure and Dynamics of Networks* (Princeton University Press, Princeton).
- Paula, D. R., Araujo, A. D., Andrade, J. S., Herrmann, H. J. & Gallas, J. A. C. [2006] “Periodic neural activity induced by network complexity,” (cond-mat 0603396), *Phys. Rev. E* **74**, 017102.
- Persson, E., Fürthauer, S., Wimberger, S. M. & Burgdörfer, J. [2006] “Transient localization in the kicked Rydberg atom,” *Phys. Rev. A* **74**, 053417.
- Poon, L. & Grebogi, C. [1995] “Controlling complexity,” *Phys. Rev. Lett.* **75**, 4023–4026.
- Rech, P. C., Beims, M. W. & Gallas, J. A. C. [2005] “Basin size evolution between dissipative and conservative limits,” *Phys. Rev. E* **71**, 017202.
- Schmidt, G. & Wang, B. W. [1985] “Dissipative standard map,” *Phys. Rev. A* **32**, 2994–2999.
- Watts, D. J. [1999] *Small Worlds* (Princeton University Press, Princeton), Chapter 7.
- Wenzel, W., Biham, Q. & Jayaprakash, C. [1991] “Periodic orbits in the dissipative standard map,” *Phys. Rev. A* **43**, 6550–6557.
- Wimberger, S. M. [2004] “Chaos and localization: Quantum transport in periodically driven atomic systems,” PhD Thesis, Ludwig-Maximilians-Universität München; Available online at [edoc.ub.uni-muenchen.de/archive/00001687](http://edoc.ub.uni-muenchen.de/archive/00001687).
- Zaslavsky, G. M. [1978] “The simplest case of a strange attractor,” *Phys. Lett. A* **69**, 145–147.
- Zou, Y., Thiel, M., Romano, M. C. & Kurths, J. [2006] “Shrimp structure and associated dynamics in parametrically excited oscillators,” *Int. J. Bifurcation and Chaos* **16**, 3567–3579.